Friedrich Schiller Universität Jena
PAF

Dissertation

High-Fluence Ion Beam Irradiation of Semiconductor Nanowires

Andreas Johannes

März 2015

Abstract

Hier alles Bla

Contents

1 Introduction **1**

2 High Doping Concentrations in Nanowires **2**

2.1 Doping and Sputtering 2

2.2 nano-XRF on single nanowires 4

2.3 Pseudo-dynamic simulation 9

2.4 Summarizing Discussion 14

3 Summary and Outlook **16**

1 Introduction

2 High Doping Concentrations in Nanowires

This chapter will discuss the concentration of dopants incorporated into ion irradiated nanowires. The simulations and experiments presented in this chapter where all performed with $175\,keV\ Mn^+$ irradiated ZnO nanowires, however, the effects are easily applied to other material combinations. Some of the first results are also published in reference [JNP+14].

2.1 Doping and Sputtering

With *iradiana* the distribution of the places where the ions come to rest gives the profile of the concentration of dopants per fluence. Locally the concentration $[{}^{atoms}/_{cm^3}]$ increases a certain amount per fluence $[{}^{ions}/_{cm^2}]$, leading to the somewhat awkward unit of for the doping efficacy $[{}^{(atoms/cm^3)}/_{(ions/cm^2)}]$. An example of the dopant distribution simulated with *iradina* is shown in figure 2.1a for the irradiation of a ZnO nanowire with $175\,keV\ Mn^+$. The ions enter the y-z plane at random locations and at an angle of 45° to the z-axis, which is periodically continued outside the plane of the image. It is clear that a homogeneous doping profile is not easy to obtain for the irradiation of a nanowire from one side. As with the creation of a box profile in bulk irradiation, multiple irradiation steps with varying energy are required. Note that an ion energy of

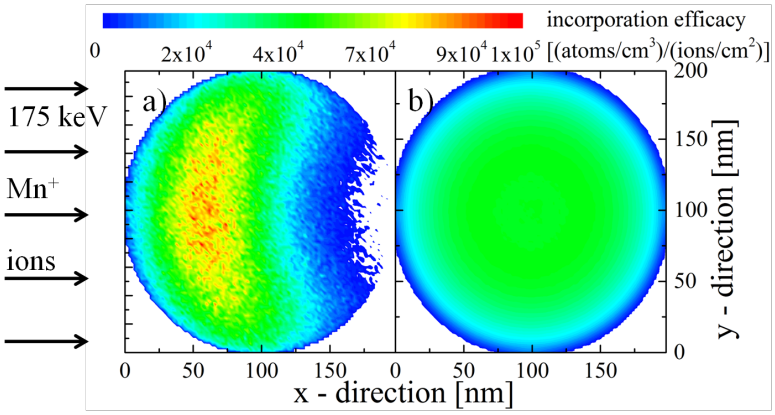

Figure 2.1: a) Color plot of the increase in concentration per fluence for the irradiation of a ZnO nanowire with $175\,keV$ Mn^+ ions at an angle of 45° to the z-axis. The energy was selected so that the rotation of this profile produces a radially homogeneous dopant distribution, as shown in b). The mean dopant incorporation efficacy is $3.6 \cdot 10^4\ {}^{(atoms/cm^3)}/_{(ion/cm^2)}$.

$175\,keV$ is obviously not enough to permeate the whole nanowire diameter of $200\,nm$, so that an additional irradiation with higher ion energy would be required to obtain homogeneous doping. Rotating the nanowire under the ion beam is a much easier way of increasing homogeneity of the doping profile. Figure 2.1b shows the local dopant incorporation efficacy for the rotation of the profile show in 2.1a. Irradiation with a single, relatively low ion energy produces a homogeneous doping profile.

As lower energy ions have lower ranges, there are fewer paths that cause the ion to leave the nanowire, particularly in the forward direction. Therefore, the first advantage of decreasing the ion energy is that the doping efficacy is larger for lower ion energies, so a lower irradiation fluence is required to achieve doping at a desired concentration. Furthermore, lower ion energy impacts also produce less damage in the irradiated matrix. Together with an optimal irradiation temperature, the rotated irradiation was utilized to improve the magnetic properties

of Mn^+ irradiated $GaAs$ nanowires in references [BMB+11, PKB+12, Bor12, KPJ+13, PKJ+14].

2.2 nano-XRF on single nanowires

The increase in doping concentration with the irradiated ion fluence was investigated on ZnO nanowire samples grown in Jena. The samples such as the one shown in figure **??**a show an upstanding, dense forest of nanowires on the growth substrate. The nanowires were transferred onto the carbon-foil of a Cu TEM grid by imprinting after the rotated irradiation with $0.24, 0.48, 0.95$ and $1.9 \cdot 10^{17}\, ^{ions}/_{cm^2}$ Mn^+ ions at $175\,keV$; corresponding to Mn/Zn ratios of $0.02, 0.04, 0.08$ and 0.16, as extrapolated from the mean doping efficacy obtained from the *iradina* simulation.

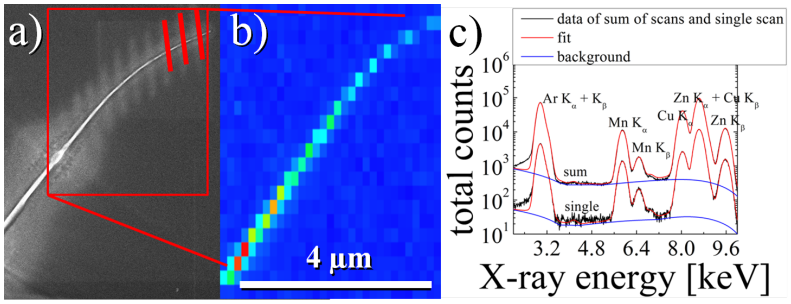

Figure 2.2: a) SEM image of a $175\,keV$ Mn^+ irradiated ZnO nanowire on the carbon-foil of a Cu TEM grid after XRF investigation. The red lines indicate where the focused X-ray beam was scanned with a long integration time. b) Intensity map of the X-ray signal. c) Exemplary XRF-spectra of a single scanned line and for the sum of all the lines for the nanowire shown in a) and b).

Figure 2.2a shows a SEM image of one of the Mn^+ irradiated ZnO nanowires after investigation by nano-XRF at the ESRF. At one point the nanowire shows some damage where the exposure to the XRF-beam was prolonged during the navigation on the sample. Also the track of the

intense, focused X-ray beam can be seen on the carbon foil by some redeposition of material. All in all, the damage to the nanowire is, however, not large enough to have an effect on the quantification, especially considering that this particular nanowire was selected because it showed the most pronounced effects. In 2.2b a map of the detected X-ray intensity clearly shows the nanowire. The XRF spectrum collected for one of the scans indicated in the SEM image 2.2a is shown in 2.2c. The number of counts for a single scan is comfortably sufficient to quantify the Mn and Zn content. The average concentration for a nanowire was determined by fitting the sum XRF-spectrum of all scans across the nanowire.

The Mn/Zn ratio is plotted over the position along the nanowire for the four nominal concentrations in figure 2.3a. Clearly there is a significant gradient in the Mn concentration along the nanowire length. The maximum Mn/Zn ratio was always found at the tip of the nanowire, the tip being identifiable in the SEM images by the slight tapering of the nanowires. The Mn/Zn ratio for both the sum of all scans, as well as the scan at the tip showing the maximum Mn/Zn ratio, is plotted in 2.3b alongside the nominal ratio extrapolated from *iradina* simulations.

Two pieces of information can be gained from these results. First, the nanowires on the sample clearly shadowed each other from the ion beam, leading to the pronounced Mn concentration gradient along the wires' length. The shadowing is least at the tips of the nanowires, therefore these points correspond closest to the simulated situation. The second point is that the increase in Mn concentration with the ion fluence is much stronger than the linear extrapolation from static simulations. The assumption underlying the doping efficacy gained from the earlier simulations and using it to calculate the required fluence for a desired doping concentration is that the concentration increases linearly with the irradiated fluence. However, this is only true in the absence of sputtering. Sputtering erodes the target nanowire at the same time as ions are in-

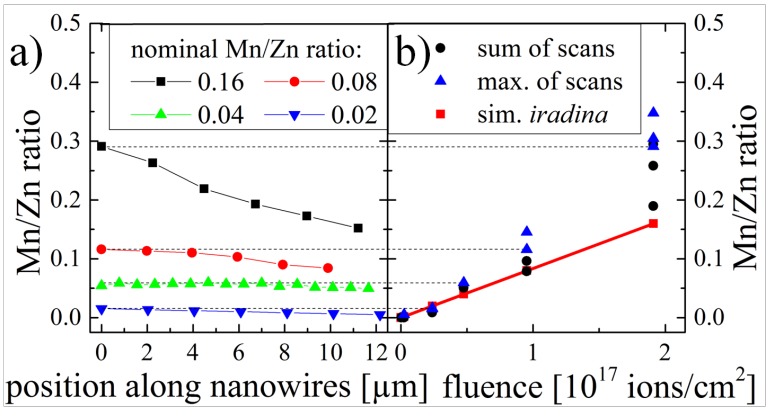

Figure 2.3: a) Mn/Zn ratio quantified with PyMCA for representative wires along the length of the nanowires for varying nominal concentrations. The corresponding data points in the plot of the concentration versus the irradiated ion fluence in b) are connected with a dashed line. The red data points and line in b) indicate the linear extrapolation to the nominal Mn/Zn ratio from *iradina* simulations. The black circles show the average ratio obtained by fitting to the sum of all scans, while the blue upturned triangles show the maximum ratio found for along the length of a nanowire.

corporated. It thus leads to a non-linear increase in the concentration of dopants with the irradiated fluence. To separate these two effects the irradiation and quantification has to be repeated with nanowires with a sparser lateral distribution, as shown in **??**b. These were kindly provided by Dr. Helena Franke from the University Leipzig.

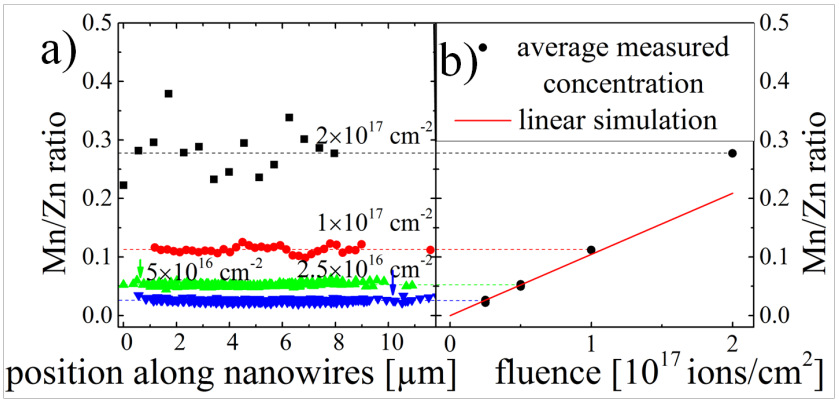

Figure 2.4: a) Mn/Zn ratio along the wire length for sparse nanowire samples irradiated with the indicated ion fluence of $175\,keV\,Mn^+$. There is no concentration profile along the wire length. In b) the black circles show the average ratio obtained by fitting to the sum of all scans for the respective ion fluence. The red line in b) shows the linear extrapolation from *iradina* simulations.

The same nano-XRF quantification procedure was followed to investigate the Mn/Zn ratio after the irradiation of these sparser nanowire samples with $0.25, 0.5, 1$ and $2 \cdot 10^{17}\,{}^{ions}/_{cm^2}$ $175\,keV$ of Mn^+. The results are shown in figure 2.4. The Mn/Zn ratios plotted against the nanowire length in 2.4a no longer show any gradient. Now we can be sure that the incorporation is not effected by the shadowing of the nanowires amongst themselves. The Mn/Zn ratio for the nanowires irradiated with higher fluences shows a significant spread due to the fact that the thinned nanowires have a much smaller volume and thus give a lower XRF signal. Added to this, the thinner wires could only be attached to

the lacy carbon loosely, so that they drifted much more during the XRF scans making it impossible to increase the integration time significantly to compensate for the lower signal.

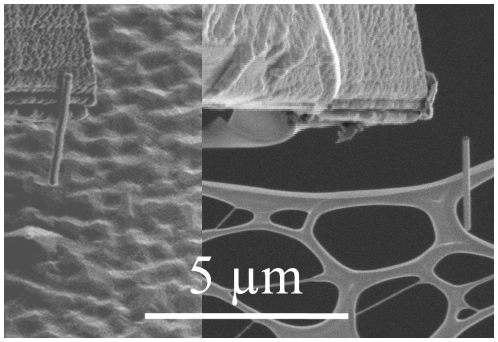

Figure 2.5: SEM images showing a ZnO nanowire broken off the growth substrate (left) and transferred onto the lacy carbon-foil on a commercial TEM grid (right). Using this technique nanowires investigated by SEM before and after the irradiation could be selected for nano-XRF quantification.

As shown in figure 2.5, these wires were individually transferred to the lacy carbon TEM grid, so they could be investigated by SEM before and after irradiation. For example, the diameter of the nanowire irradiated with the highest fluence was reduced from $202\,nm$ to $93\,nm$ by sputtering. The nanowires irradiated with lower fluences showed lower reductions in their diameters, as expected. From these diameter reductions the sputter yield can again be calculated, yielding values in the range of 5 - 20. As seen in the dedicated study on sputtering these values have a very large spread.

The average Mn/Zn ratio is plotted in 2.4b against the irradiated fluence for all irradiated fluences. It is accurate to within $\pm\,0.01$, as it is based on the sum of the spectra of all the individual scans. This sum-spectrum includes a sufficiently large number of counts in all instances. The initial increase in the Mn/Zn ratio with the irradiated ion fluence closely follows the the linear extrapolation from the doping efficacy for fluences up to $0.5 \cdot 10^{17}\,{}^{ions}/_{cm^2}$. This is an important result, as it confirms that the MC BCA simulation can accurately predict the incorporation of dopants quantitatively. Therefore the doping efficacy is a useful number

to determine the required ion fluence for a desired doping concentration for low fluences, were sputtering is not yet significant. However, as with the denser nanowire sample, for high fluences the increase in the Mn concentration is much larger than the simple linear extrapolation from the *iradina* simulation.

2.3 Pseudo-dynamic simulation

The direct simulation of the effect of sputtering on the incorporation of dopants into nanowires requires a dynamic simulation program which also considers the three dimensional geometry of the target. As such software is not currently openly available, a step-by-step investigation using results from static simulations will be undertaken to discuss the observed interaction between dopant incorporation and sputtering.

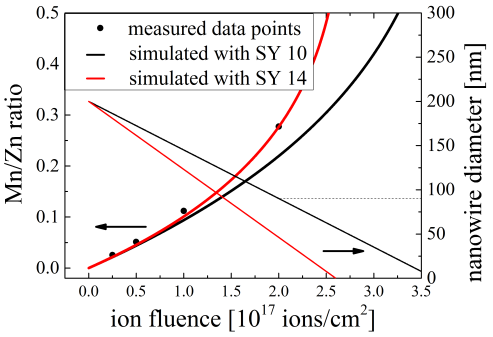

Figure 2.6: Plot of the Mn/Zn ratio (left axis) versus the irradiated ion fluence of $175\,keV\,Mn^+$ for the measured nanowires and two simulations, indicated by black circles, a black line and a red line respectively. The nanowire diameter (right axis) is also plotted against the fluence for both simulations. The dashed line at $90\,nm$ marks the final radius of the data point corresponding to the highest irradiated fluence.

The most straightforward approach is to consider the total sputter yield and the doping efficacy to be constant. With these assumptions and a reiterative calculation of incremental fluence steps, a pseudo-dynamic simulation can be numerically constructed. The Mn concentration increases with each irradiated incremental fluence step by the value de-

termined by the doping efficacy. Then the number of Zn, O and Mn atoms is reduced by sputtering in such a way, that the total sputter yield is divided between $Zn + O$ and Mn according to the current Mn concentration. The total number of atoms is used to calculate the new nanowire radius and the next incremental fluence step can be calculated. Figure 2.6 shows the experimentally determined Mn/Zn ratios next to such a simulation. The doping efficacy was set to the same value used for the linear extrapolation so far: $3.6 \cdot 10^4 \, {}^{(atoms/cm^3)}/_{(ion/cm^2)}$. The total sputter yield was set to 10 for the simulation yielding the values depicted in black. This sputter yield value corresponds to the sputter yield determined from the reduction in the radius of the nanowire irradiated with $2 \cdot 10^{17} \, {}^{ions}/_{cm^2}$ and therefore, unsurprisingly, this simulation produces the the correct diameter of $\approx 90\,nm$ at this ion fluence. However, the calculated Mn/Zn ratio is too low. Conversely, a simulation with a larger sputter yield of 14, indicated in red, correctly reproduces the Mn/Zn ratio, but erodes the nanowire too quickly. Nevertheless, the overall agreement between the experiment and the simulation seems promising and confirms that the super linear increase in the doping concentration observed in the experiment can be explained by the sputtering of the nanowire.

To increase the accuracy of the pseudo-dynamic simulation, results from a set of static simulations for varying diameters can be used. The sputter yield is dependent on the nanowire radius and the ion energy as shown in 2.7a and 2.7c. This relation is discussed in detail in the previous chapter **??**. Likewise, the incorporation efficacy plotted in 2.7b is also dependent on the nanowire radius and the ion energy. For a fixed diameter and increasing ion energy the efficacy is monotonically decreasing, as the probability of the ion to leave the nanostructure rises together with the ion range. For a fixed ion energy, as shown in figure 2.7d, the probability of an ion to stay in the nanostructure increases with

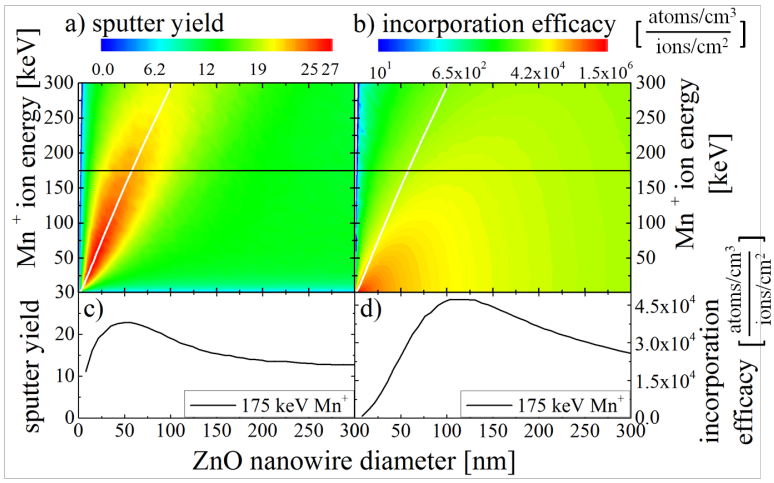

Figure 2.7: a) Sputter yield for the irradiation with Mn^+ of ZnO nanowires with varying diameters an ion energies. From the same simulations the dopant incorporation efficacy was determined and plotted in b). The white line in both plots indicates the ion range at the respective energy and 45°, calculated with SRIM for Mn^+ in ZnO. The horizontal black line indicates the ion energy used in the experiments and simulations in this chapter. For this energy the diameter dependent sputter yield and doping efficacy are plotted in c) and d) respectively.

increasing nanowire diameter, so that for small diameters the efficacy also increases with increasing diameter. For large diameters this effect is overcompensated by a stronger dilution of the dopants in the volume of the nanowire which increases as the square of the diameter. This leads to a maximum in the incorporation efficacy at diameters around twice the ion range. Note that the color scale in 2.7b is logarithmic, while the graph 2.7d has a linear scale.

The numerical, pseudo-dynamic simulation can easily be adapted to use the diameter dependent values for the sputter yield and the dopant incorporation efficacy of figures 2.7c and 2.7d. As with the previous pseudo-dynamic simulation, which only considered constant sputtering and dopant incorporation efficacy, it is only possible to reproduce the correct diameter or the Mn/Zn ratio. For the results shown in 2.8 the diameter dependent sputter yield used for the simulation had to be halved. A simulation with the full sputter yield shown in figures 2.7c already eroded the $200\,nm$ nanowire completely after the irradiation with an ion fluence of $\approx 1.5 \cdot 10^{17}\,{}^{ions}/_{cm^2}$. This is not a cause for concern, however, because the quantitative values for the sputter yield obtained by *iradina* simulations are not expected to be reliable and the effective sputter yield will be reduced in a material which can (re)-oxidize. Both these points were already discussed in chapter **??**.

The resulting Mn/Zn ratios from such a simulation are plotted in figure 2.8 as red squares. The stronger than linear increase in the Mn/Zn ratio with the irradiated ion fluence continues for low ion fluences until the doping efficacy starts decreasing markedly with decreasing diameter from diameters around $100\,nm$. At this diameter, the $175\,keV\,Mn^+$ ions start to reach the back of the now thinned nanowire, the sputtering increases and the doping efficacy decreases, as shown in figures 2.7c and 2.7d. In the evolution of the diameter with the irradiated ion fluence,

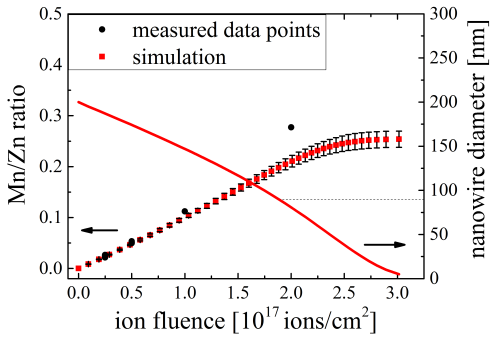

Figure 2.8: Results from a pseudo-dynamic simulation considering diameter dependent sputtering and doping efficacy. The Mn/Zn ratio is plotted to the left axis versus the ion fluence of $175\,keV\,Mn^+$ as red squares for the simulation and black circles for the experiment. The error bars range from the Mn/Zn ratio for $170\,keV$ to $180\,keV\,Mn^+$. The red line indicates the simulated nanowire diameter.

plotted in figure 2.8 as a red line, the increased sputter yield is noticeable as a slight increase in the slope of the curve at $2 \cdot 10^{17}\,{}^{ions}/_{cm^2}$.

Largely due to the reduced Mn incorporation in thinned nanowires, the simulation fails to reproduce the measured Mn/Zn ratio for ion fluences of $1 \cdot 10^{17}\,{}^{ions}/_{cm^2}$ and above, underestimating the Mn concentration significantly. This is due to the assumption that the probability of sputtering a Mn or a Zn/O atom is determined by the average Mn concentration in the nanowire. This would only be true if the doping profile were truly homogeneous. In reality there is a Mn poor surface region in the doping profile shown in figure 2.1b. In addition, as the nanowire is thinned during the irradiation, the homogeneity of the doping profile will also suffer. A peak emerges in the middle of the nanowire as the radius becomes equal to the ion range and smaller. In summary this means that more Zn and O atoms are sputtered from the nanowire than predicted by the Mn concentration weighted sputter yield and that the core is enriched in Mn slightly faster than the averaged doping incorporation efficacy would suggest. When the outer Mn poor layers of the nanowire are sputtered away the Mn/Zn ratio averaged over the whole cross-section increases, even without the additional incorporation

of Mn. At this point it no longer makes sense to try to predict doping concentrations with static simulations which cannot take into account the change in the target composition and geometry. Dynamic simulations are required.

2.4 Summarizing Discussion

The incorporation of dopants into nanowires was studied by investigating Mn irradiated ZnO nanowires with nano-XRF. The first, perhaps slightly obvious result is that the doping concentration can be significantly influenced by shadowing of the nanowires amongst themselves. *Ronning + Sebastian ? []* Preventing the shadowing of the ion beam sets some limits on suitable samples for irradiation. Related to this fact is the insight that control of the irradiation geometry, such as the possibility of irradiation from different angles, in the presented case by rotation of the target, can greatly reduce both the energy and ion fluence required to obtain a certain doping concentration. Both a reduced energy and a reduced ion fluence reduce the total damage produced in the target and can elevate the annealing requirements [BMB+11, PKB+12, Bor12, KPJ+13, PKJ+14]. In any case, it was already shown that irradiated nanowires can bend in either direction relative to the ion beam, depending on the ion energy [BSL+11]. The rotated irradiation is the only alternative to complex modulations of the ion energy to prevent this bending during the irradiation with high fluences in materials that show such bending.

The quantification of the dopants in irradiated nanowires showed that the static MC BCA code *iradina* is accurate in the prediction the doping concentration for low ion fluences. This was expected from the discussion in chapter **??** on the underlying scientific background for the direct

simulation of ion trajectories which translates well into nanostructures and thus gives an accurate prediction of the final distribution of the ions in the target. However, a reasonable upper limit to the applicability of static simulations seems to be given in these experiments by a fluence of $0.5 \cdot 10^{17}\,{}^{ions}/_{cm^2}$. This corresponds to the reduction of the nanowires diameter by about 10%, or a reduction of the nanowire volume by roughly 20%. Note, that this result can be generalized to other nanowires, ion species and ion energies only if the ion range is comparable or larger than the nanowire diameter. For low ion energy irradiation, where the ion range is also low, the sputtering will effect the doped volume of the nanowire much sooner! In layered samples ... TODOWolfhard Möller tridyn? []

Unfortunately there is no straightforward way to extend the usefulness of static simulations to higher ion fluences. Although the attempted pseudo-dynamic simulations were able to reproduce the incorporated doping concentration or the nanowire radius, this was only possible in retrospect and by altering the simulation parameters. A predictive algorithm that is not dynamic was not found. The problem caused by the inhomogeneous incorporation of the dopant and the disproportionately large sputtering of the nanowire material can be solved by dynamic codes which consider both the nanostructure geometry as well as the local concentration of each element. A remaining problem is posed by the sputter yield which is not a priori easy to simulate correctly. This was discussed in chapter **??** on sputtering, but is significantly compounded by the possibility of preferential sputtering of specific elements. Again, this has already been investigated in flat geometries //

3 Summary and Outlook

check: Master Thesis Noack, Ogrisek, Conference proceding D. Sage, Rutherford, Nordlund

Bibliography

[BMB+11] Christian Borschel, Maria E. Messing, Magnus T. Borgstrom, Waldomiro Paschoal, Jesper Wallentin, Sandeep Kumar, Kilian Mergenthaler, Knut Deppert, Carlo M. Canali, Hakan Pettersson, Lars Samuelson, and Carsten Ronning. A New Route toward Semiconductor Nanospintronics: Highly Mn-Doped GaAs Nanowires Realized by Ion-Implantation under Dynamic Annealing Conditions. *Nano Letters*, 11(9):3935–3940, September 2011. WOS:000294790200073.

[Bor12] Christian Borschel. *Ion-Solid Interaction in Semiconductor Nanowires*. PhD thesis, University Jena, Jena, 2012.

[BSL+11] Christian Borschel, Susann Spindler, Damiana Lerose, Arne Bochmann, Silke H. Christiansen, Sandor Nietzsche, Michael Oertel, and Carsten Ronning. Permanent bending and alignment of ZnO nanowires. *Nanotechnology*, 22(18):185307, May 2011. WOS:000288653300010.

[JNP+14] A. Johannes, S. Noack, W. Paschoal, S. Kumar, D. Jacobsson, H. Pettersson, L. Samuelson, K. A. Dick, G. Martinez-Criado, M. Burghammer, and C. Ronning. Enhanced sputtering and incorporation of Mn in implanted GaAs and ZnO nanowires. *Journal of Physics D-Applied Physics*, 47(39):394003, October 2014. WOS:000341772000005.

[KPJ+13] Sandeep Kumar, Waldomiro Paschoal, Andreas Johannes, Daniel Jacobsson, Christian Borschel, Anna Pertsova, Chih-Han Wang, Maw-Kuen Wu, Carlo M. Canali, Carsten Ronning, Lars Samuelson, and Håkan Pettersson. Magnetic Polarons and Large Negative Magnetoresistance in GaAs Nanowires Implanted with Mn Ions. *Nano Letters*, 13(11):5079–5084, 2013.

[PKB+12] Waldomiro Paschoal, Sandeep Kumar, Christian Borschel, Phillip Wu, Carlo M. Canali, Carsten Ronning, Lars Samuelson, and Hakan Pettersson. Hopping Conduction in Mn Ion-Implanted GaAs Nanowires. *Nano Letters*, 12(9):4838–4842, September 2012. WOS:000308576000069.

[PKJ+14] W. Paschoal, Sandeep Kumar, D. Jacobsson, A. Johannes, V. Jain, C. M. Canali, A. Pertsova, C. Ronning, K. A. Dick, L. Samuelson, and H. Pettersson. Magnetoresistance in Mn ion-implanted GaAs:Zn nanowires. *Applied Physics Letters*, 104(15):153112, April 2014. WOS:000335145200060.